International Journal of Environmental Sciences
ISSN: 2229-7359
Vol. 10 No. 6s, 2024
https://theaspd.com/index.php

Next-Generation Dual-Band MIMO Antenna with Slot Integration for 5G and Satellite Communication

Kamal Prakash Pandey[1], Rakesh Kumar Singh[2], Surya Bhushan Dubey[3], Mohd Khalid[4], Amrees Pandey*[5]

[1]Department of Electronics and Communication Engineering, BBS College of Engineering and Technology, Prayagraj, Uttar Pradesh, India
[2, 5]Department of Electronics and Communication Engineering, Shambhunath Institute of Engineering and Technology (SIET), Prayagraj, Uttar Pradesh, India
[3]Department of Electrical and Electronics Engineering, S. R. Institute of Management and Technology, Lucknow, Uttar Pradesh, India
[4]Department of Electronics and Communication, University of Allahabad, Prayagraj, Uttar Pradesh, India
pandeykamal.1976@gmail.com[1] , rksingh_rakesh@yahoo.com[2] , suryadubey1@gmail.com[3] , mohd.khalid.411@gmail.com[4] , amrishpandey19@gmail.com[5]
*Corresponding Author Email: amrishpandey19@gmail.com

Abstract: *This work presents a novel spiral-shaped microstrip patch 2×2 MIMO antenna designed for 5G (n258 band) and satellite communication applications. The proposed antenna (A4) employs a dual-band parallel port arrangement, which effectively enhances isolation to better than 30 dB. It achieves an impedance bandwidth of 31.79% (19.82–27.31 GHz) and 14.23% (31.07–35.83 GHz), corresponding to resonant frequencies at 26.29 GHz and 32.64 GHz, respectively. The radiating element integrates a meandered-shaped slot between ports, significantly improving bandwidth, peak gain, and isolation. The compact antenna occupies a total size of 30 × 30 × 1.6 mm³, making it highly suitable for modern wireless systems. To evaluate diversity performance, key MIMO parameters such as Envelope Correlation Coefficient (ECC), Diversity Gain (DG), Total Active Reflection Coefficient (TARC), and Channel Capacity Loss (CCL) are analyzed. Both simulated and measured results validate the antenna's superior performance and confirm its effectiveness for next-generation high-frequency communication systems.*

Index Terms: *MIMO, 5G, Isolation, Radiation Pattern, ECC, CCL*

1. INTRODUCTION

In recent years, compact UWB (Ultra-Wideband) and wideband MIMO antennas have gained significant attention in modern wireless communication systems due to their simple design, low fabrication cost, high throughput, and wide resonance frequency coverage [1–2]. The adoption of MIMO (Multiple-Input Multiple-Output) technology has further enhanced system performance by offering high data rates, improved reliability, and better spectral efficiency, which are crucial for present and next-generation wireless networks [2–3]. When MIMO and UWB technologies are integrated with parallel transmission and multipath propagation of multiple signals, substantial diversity and multiplexing advantages can be achieved [3]. Consequently, MIMO antennas have emerged as an essential research area for engineers in wireless communication [4]. A major challenge in wireless communication is multipath fading, which occurs due to reflection, refraction, and scattering of electromagnetic waves in free space [5–6]. This issue can be mitigated using polarization diversity or frequency diversity techniques. However, to ensure optimum system performance, there is a strong need for compact MIMO antenna structures that exhibit low inter-element mutual coupling without compromising bandwidth [7].

On the other hand, while wideband antennas provide broad frequency coverage, they often suffer from reduced isolation between elements and higher envelope correlation, leading to performance degradation and increased antenna size [7]. Therefore, achieving a compact, wideband MIMO antenna with high isolation and low ECC is a key design challenge. Although MIMO antennas offer high data rates compared to conventional SISO systems, they often suffer from narrow bandwidth and mutual coupling

issues. To address this, several isolation enhancement techniques have been reported in literature, including meta-surfaces, diversity techniques, and neutralized lines [8–14]. Wideband MIMO antennas have also been proposed for multiple applications [15–16]. For instance, Singh et al. [17] reported a modified 2×2 flare horn-shaped MIMO antenna with improved isolation, while Singh et al. [18] designed a dual-port circular-shaped MIMO antenna for Ku/K-band applications. Similarly, a circularly polarized spidron fractal patch antenna for Ku-band [19], a 4×4 fractal circular ring radiator for UWB [20], and a two-port MIMO antenna with parasitic reflectors [21] have been presented. Other contributions include a tri-forked compact MIMO antenna for radar applications [22], a four-port hammer-shaped CP antenna for K-band [23], a super-wideband MIMO antenna for S, C, X, K, and Ka bands [24], and compact MIMO antennas for 5G NR (n257/n258/n261) bands [25]. The performance of the proposed design is benchmarked against existing literature (Table-1), comparing key parameters such as operating band, substrate, peak gain, isolation, ECC, DG, CCL, and antenna size. The proposed antenna, with a compact dimension of 30 × 30 × 1.6 mm³, demonstrates superior results, including a peak gain of 5.8 dBi and 5.2 dBi, and an isolation level of –30 dB, which outperforms many existing designs [26–38].

Table.1 Comparative analysis with modern literature

Ref	Antenna Size (in mm^3)	Operating bands/BW (GHz)	Gain (dBi)	Isolation (dB)	ECC	DG	CCL	Applications
26	30×35×0.76	24.25-27.5/3.25	8.3	<-15	<0.10	>9.96	Nil	K band, Wideband
27	35×40×1.6	25.5-29.6)/4.1	5.34	<-20	<0.08	>9.99	0.4	Ka band, Wideband
28	29×60×1.6	3-20/17	3.7	<-23	<0.01	>9.99	0.32	C, X, Ku
29	50×30×1.6	2.5-14.5/12	4.3	<-20	<0.04	>7.4	Nil	C, X, Ku
30	32×32×1.6	15.64-17.45/1.8 17.87-18.99/1.5 19.31-21.13/1.8 22.14-23.79/1.6	2.4 3.4 5.8 1.1	<-22	<0.05	>9.97	Nil	K band, Wideband
31	32×32×1.6	14.30-15.31/1 16.83-18.59/1.7 19.19-23.44/4.2 25.37-27.89/2.5 31.02-33.82/2.8	1.9 5.25 1.6 4.3 2.2	<-17	<0.08	>9.97	Nil	Ku, K, Ka
32	55×50×1.6	15.31-20.02/4.7	7.5	<-20	<0.05	>9.99	11.34	Ku, K
33	55.6×50.5×1.6	1.5-40/38.5	7.5	<-20	<0.05	>9.99	0.35	UWB
34	50×40×1.6	2.5-11/8.5	2.11	<-15	<0.01	Nil	Nil	UWB
Present Work	**30×30×1.6**	**19.82-27.31/7.4 31.07-35.83/4.7**	**5.8 5.2**	**<-30**	**<0.04**	**>9.98**	**0.21**	**Wideband, UWB**

In this research, we propose a novel spiral-shaped wideband MIMO antenna optimized for radar and satellite communication applications. The antenna is fabricated on an FR-4 substrate (εr = 2.20, tan δ = 0.0009, thickness = 1.6 mm), featuring a compact structure with excellent isolation and diversity performance. The key outcomes of the proposed design are as follows:

a. Compact and Cost-Effective Design

The dual-port MIMO antenna (A4) is highly miniaturized and economical. Both simulated and measured results confirm its effectiveness. The antenna covers 19.82–27.31 GHz (K-band: 18–26.25 GHz) and

31.07–35.83 GHz (Ka-band: 26.5–40 GHz), making it suitable for radar and satellite applications.

b. High Isolation and Bandwidth Enhancement

The parallel arrangement of radiating elements with a meandered slot between ports ensures an impedance bandwidth of 31.79% (19.82–27.31 GHz) and 14.23% (31.07–35.83 GHz). Exceptional isolation better than 30 dB is achieved at resonant frequencies of 26.29 GHz and 32.64 GHz, ensuring minimal correlation between signals.

c. Superior Diversity Performance

The antenna achieves excellent diversity parameters with ECC < 0.04, DG > 9.8 dB, and CCL<0.21 bps/Hz, confirming its suitability for high-capacity, interference-free communication. A fabricated prototype and corresponding measurements validate the simulation results.

2. ANTENNA DESIGN AND PARAMETRIC ANALYSIS

A compact dual-element MIMO antenna has been designed and fabricated on a low-cost FR-4 epoxy substrate ($\varepsilon_r = 2.20$, $\tan\delta = 0.0009$, thickness = 1.6 mm). The antenna configuration consists of radiating elements and a ground plane, which are carefully optimized to validate the simulated results. The detailed geometrical specifications of the proposed antenna are listed in Table-2. The antenna layout comprises two sections: the upper part (red region) representing the radiating patch and the lower part (green region) corresponding to the ground plane, both excited through a 50 Ω microstrip feed line, as illustrated in Figure 1. The step-by-step evolution of the antenna geometries (A1 to A4) is depicted in Figure 3, showing the progressive improvements incorporated into the final design. The fabricated prototype is presented in both top and bottom views in Figure 2, and all experimental measurements were conducted using a Schwarz Vector Network Analyzer (ZNB40), operating across 10 MHz to 40 GHz. Furthermore, a detailed parametric analysis of the radiating element and ground structure was carried out, governed by the standard design equations (1)–(6) [27–31]. The patch width (W) of the antenna was calculated using the following fundamental expression:

$$W = \frac{c}{2f}\sqrt{\frac{2}{\varepsilon_{r+1}}} \tag{1}$$

Where, ε_r is the dielectric constant of substrate and f is the center frequency, Length of patch is calculated by the equation:

$$L = L_{ef} - 2\Delta l \tag{2}$$

$$L_{ef} = \frac{c}{2f\sqrt{\varepsilon_{re}}} \tag{3}$$

Where L_{ef} is the Patch effective length and ε_{re} is the effective substrate dielectric constant is given by;

$$\varepsilon_{re} = \frac{\varepsilon_{re}+1}{2} + \frac{\varepsilon_r - 1}{2}\left[1 + \frac{12h}{W}\right]^{-1/2} \tag{4}$$

Where, h is the thickness of substrate and the normalized extension in length (Δl) is given by:

$$\Delta l = 0.412\ h\frac{(\varepsilon_{re}+0.3)\left(\frac{W}{h}+0.8\right)}{(\varepsilon_{re}-0.25\ B)\left(\frac{W}{h}+0.8\right)} \tag{5}$$

Feed line length (L_f) is considered by using below equation.

$$L_f = \lambda_g/2 \tag{6}$$

Table.2: Dimensions of the proposed patch antenna

Element	Value (mm)
Substrate (Length × Width)	30 × 30
Radiating Patch (Square, L × W)	10 × 10
Slot (Square, L × W)	6 × 6
Meandered Line (L × W)	1 × 10
Radiating Patch (Rectangle, L × W)	7 × 2
Distance between Radiating Square Patches	3.5

The resonance characteristics of the proposed dual-port MIMO antenna are validated through an equivalent circuit model, as illustrated in Figure 1(b)**.** In this model, the 50 Ω load is represented by the series arrangement of L1, C1, and R1, while the proposed patch element is modeled using the series combination of L2, C2, and R2. The mutual coupling effect between Port 1 and Port 2 is accounted for by an additional series network comprising L4 and C4 [31]. Furthermore, the parallel arrangement of L3, C3, and R3 effectively represents the contribution of the meandered slot lines introduced in the design [4]. A strong correlation is observed between the equivalent circuit response and the full-wave simulated results, thereby confirming the accuracy and effectiveness of the proposed equivalent circuit model in predicting the antenna's resonance behavior.

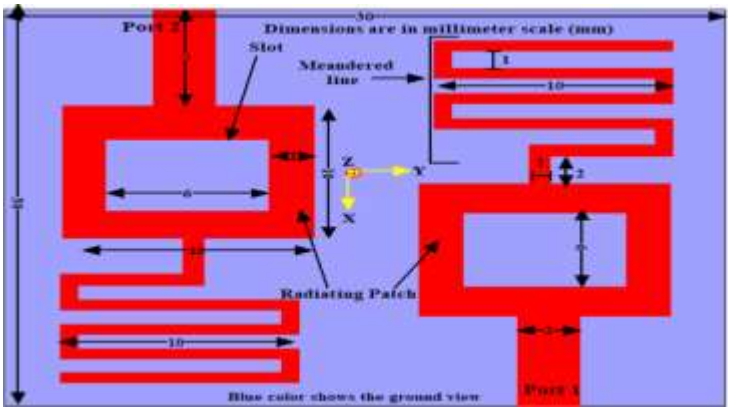

(a)

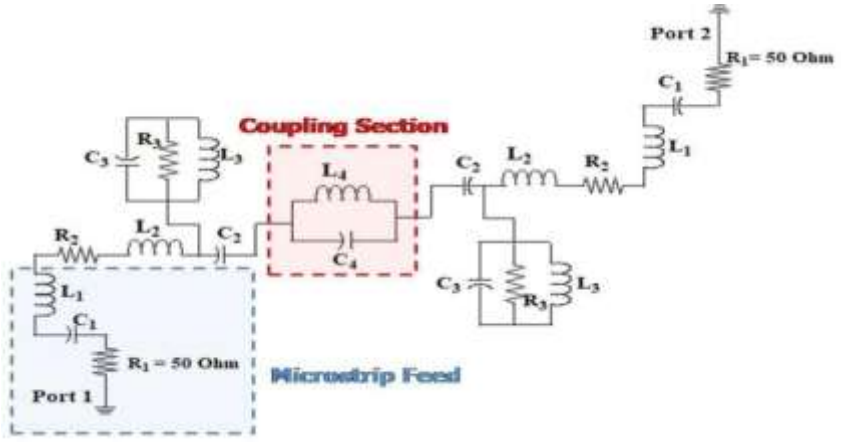

(b)

Figure 1. (a) Top view of the proposed antenna geometry, illustrating the radiating patch and ground structure. (b) Equivalent circuit model of the dual-port MIMO antenna, representing the resonance behavior and mutual coupling effects.

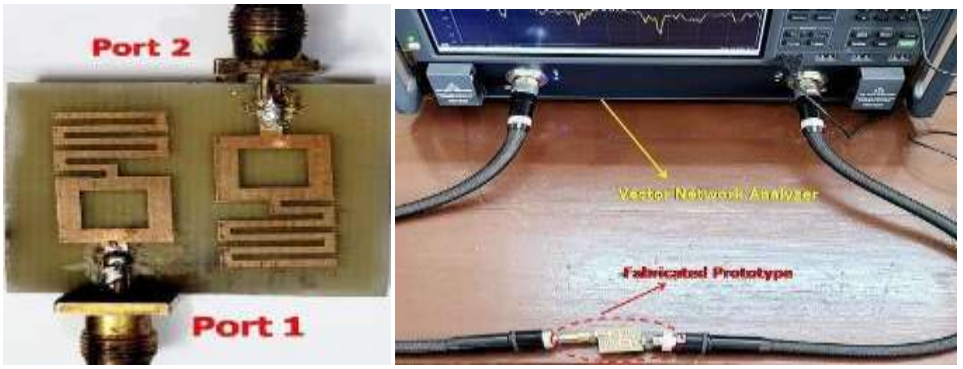

(a) (b)

International Journal of Environmental Sciences
ISSN: 2229-7359
Vol. 11 No. 22s, 2025
https://theaspd.com/index.php

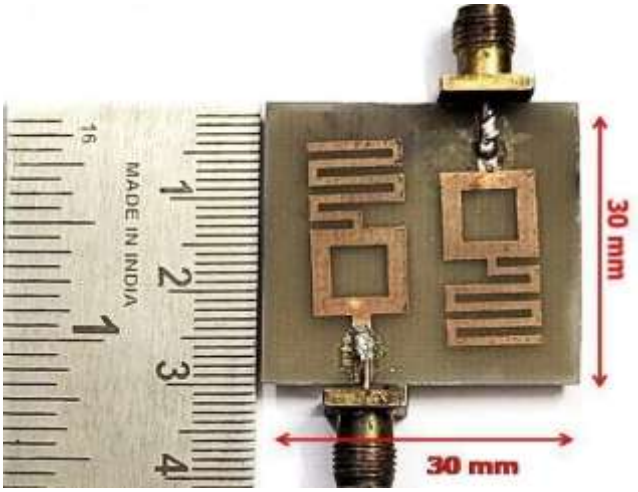

(c)

Figure 2. (a) Top view of the fabricated antenna prototype. (b) Measurement setup using the Vector Network Analyzer (VNA). (c) Physical dimensions of the fabricated MIMO antenna.

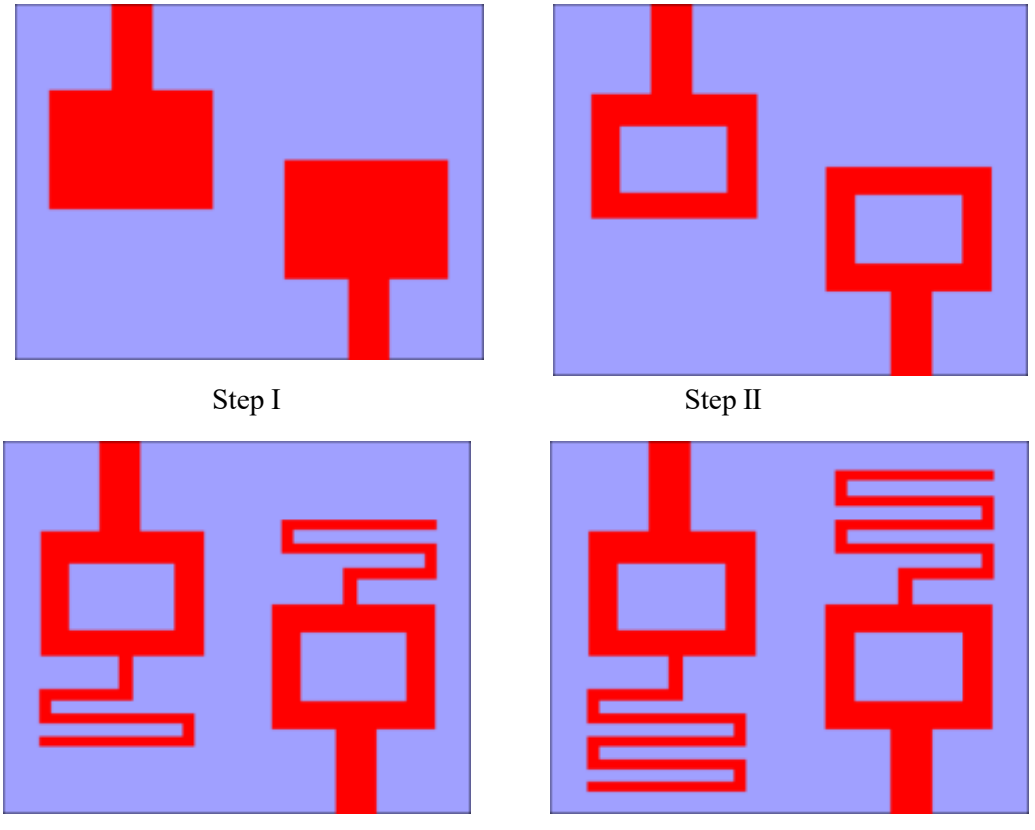

Figure 3. Step-by-step evolution of the proposed antenna geometry: (A1) basic square patch, (A2) square patch with central slot, (A3) slot-loaded patch with meander lines, and (A4) final optimized design with additional meander lines and parallel arrangement.

The design procedure of the proposed antenna is carried out in successive stages using ANSYS HFSS, commercially available electromagnetic simulation software. To illustrate the operating principle, the antenna evolution is analyzed from A1 to A4, where each step progressively improves bandwidth, mutual coupling, and polarization diversity.

- Step I (Antenna A1): A square-shaped radiating patch (10 × 10 mm²) is introduced as the basic antenna structure.

- Step II (Antenna A2): A square slot (6 × 6 mm²) is etched at the center of the radiating patch in A1, leading to enhanced impedance matching and modified current distribution.
- Step III (Antenna A3): Two meandered slots (1 × 10 mm²) are incorporated into A2, further improving bandwidth and isolation compared to A1 and A2.
- Step IV (Proposed Antenna A4): The final antenna is derived from A3 by adding additional meandered lines and introducing a parallel arrangement of elements, which facilitates polarization diversity.

The A4 configuration plays a pivotal role in achieving wide impedance bandwidth across the target frequency ranges, along with excellent isolation (> 30 dB) between the elements. Compared to its predecessors, the proposed antenna exhibits higher element separation, improved peak gain, and UWB/wideband characteristics. As a dual-port design, A4 successfully provides both polarization diversity and pattern diversity, making it highly suitable for advanced MIMO applications.

3. RESULTS AND DISCUSSION

The proposed antenna (A4) was fabricated on a low-cost FR-4 epoxy substrate (ε_r = 2.20, tan δ = 0.0009, thickness = 1.6 mm) and experimentally tested to validate the simulated performance. A Schwarz Vector Network Analyzer (ZNB40) was employed to measure the scattering parameters, while an anechoic chamber was used for the measurement of peak gain and radiation patterns. It is observed that the measured results exhibit excellent agreement with the simulated outcomes, including the reflection coefficient, mutual coupling, gain, VSWR, TARC, and CCL. This confirms the accuracy and robustness of the proposed design. Furthermore, Table 3 presents the simulated values of impedance bandwidth (IBW), resonant frequencies, reflection coefficient, and gain across the desired operating bands for all antenna stages (A1–A4) at both Port-1 and Port-2.

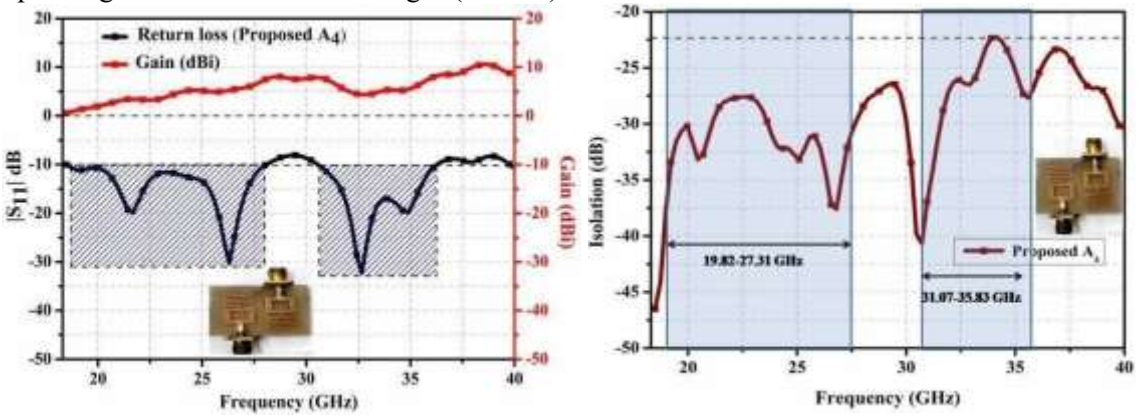

(a) (b)

Figure 4. (a) Simulated and measured return loss (S_{11}) and gain of the proposed antenna. (b) Isolation (S_{21}) versus frequency characteristics of the proposed dual-port MIMO antenna.

A spiral-shaped microstrip patch MIMO antenna with dual-band characteristics is proposed. The antenna performance has been evaluated in terms of reflection coefficient, mutual coupling, gain, TARC, VSWR, and CCL. Table 3 presents the comparative analysis of antennas A1 to A4, clearly demonstrating the dual-band operation. The tabulated data highlight impedance bandwidth (%), resonant frequency (GHz), reflection coefficient (dB), and peak gain (dBi) for both ports (Port-1 and Port-2), providing a ready reference for performance comparison. The final proposed MIMO configuration (Antenna A4) adopts a parallel arrangement (see Fig. 4). The simulated |S11| parameters reveal dual resonances at 26.29 GHz and 32.64 GHz, with corresponding impedance bandwidths of 31.79% (19.82–27.31 GHz) and 14.23% (31.07–35.83 GHz). The antenna achieves peak gains of 5.8 dBi and 5.2 dBi at the two resonant frequencies, respectively. Furthermore, the mutual coupling between the parallel-placed ports, expressed as |S21|, remains better than –30 dB across the operating bands (cf. Fig. 4b). This excellent isolation, combined with efficient impedance matching, ensures reliable operation for medium, UWB, and wideband applications.

The simulated and measured reflection characteristics of all antenna configurations (A1-A4) are depicted in Fig. 5(a, b). For the proposed MIMO antenna (A4), the simulated |S11| response indicates dual

resonances at 19.82–27.31 GHz and 31.07–35.83 GHz, while the measured |S11| response confirms slightly shifted bands of 20.11–27.21 GHz and 31.82–34.93 GHz. The impedance bandwidth is 31.79% (simulated) and 29.51% (measured) for the first band, and 14.23% (simulated) and 13.89% (measured) for the second band, both remaining below 10 dB. The |S22| parameters exhibit a similar performance trend, validating the dual-band operation for both ports.

Table 3. Comparative performance overview of the proposed antenna designs (A1–A4)

Antenna	Port NO	Number of Bands	Operating band (GHz)/ Impedance BW (in %)	Isolation (dB)	Resonant Frequency (GHz)	Reflection Coefficient (dB)	Peak Gain (dBi)
A1	Port 1	1	25.1 2- 28.12/11.26	<-20	26.12	-16.12	5
		2	33.12-36.21/8.91	<-25	34.21	-10.88	4.8
	Port 2	1	25.12-28.12/11.26	< -21	26.12	-16.12	4.9
		2	33.12-36.21/8.91	<-24	34.21	-10.88	4.8
A2	Port 1	1	25.10-26.89/6.88	<-26	25.29	-12.11	3.8
		2	27.21-30.51/11.43	<-26	26.01	-12.10	3.6
		3	33.21-37.51/12.1	<-26	35.42	-16.27	4.6
	Port 2	1	25.10-25.89/5.88	<-25	25.29	-12.11	3.8
		2	27.21-30.01/11.12	<-26	26.01	-12.10	3.6
		3	33.21-37.51/12.1	<-26	35.42	-16.27	4.6
A3	Port 1	1	25.11-26.55/5.57	<-24	25.32	-25.01	3.6
		2	30.28-31.93/5.30	<-25	30.55	-10.98	5.3
	Port 2	1	25.11-26.32/5.17	<-23	25.32	-25.01	3.9
		2	30.28-31.93/5.30	<-24	30.55	-10.98	5.1
A4	Port 1	1	19.82-27.31/31.79	<-30	26.29	-29.01	5.8
		2	31.07-35.83/14.23	<-30	32.64	30.23	5.2
	Port 2	1	19.82-27.31/31.79	<-28	26.29	-29.03	5.7
		2	31.07-35.83/14.23	<-30	32.64	30.23	5.3

Isolation characteristics are shown in Fig. 5(c). The proposed A4 antenna consistently achieves isolation better than 30 dB in both simulated and measured results. Minor deviations in the measured data can be attributed to fabrication tolerances and slight inconsistencies in the dielectric substrate. Overall, the strong agreement between simulation and experimental results confirms the suitability of the proposed MIMO antenna for high-frequency dual-band and wideband wireless applications.

The simulated and measured scattering parameters between adjacent ports indicate that the reflection coefficients |S11| and |S22| gradually decrease below 10 dB, covering the entire operating frequency range. Similarly, the isolation between the adjacent ports, represented by |S21| and |S12|, gradually

increases and remains better than –20 dB, as observed in Figure 6(a). The corresponding gain performance of the proposed MIMO antenna is presented in Figure 6(b), showing both simulated and measured values.

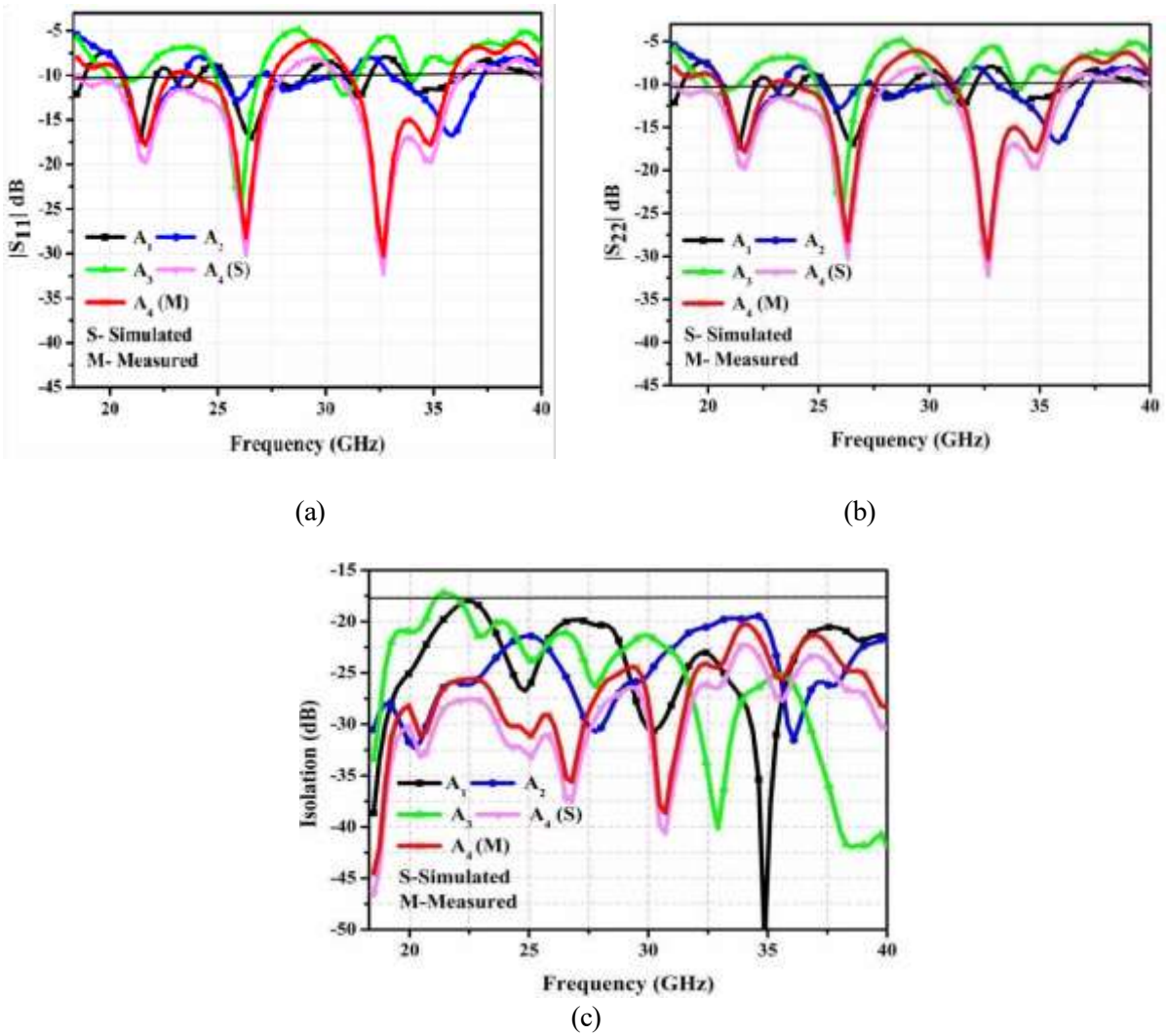

(a) (b)

(c)

Figure 5. Parametric analysis with measured results: (a) Reflection coefficient ($|S_{11}|$), (b) Reflection coefficient ($|S_{22}|$), and (c) Isolation characteristics as a function of frequency.

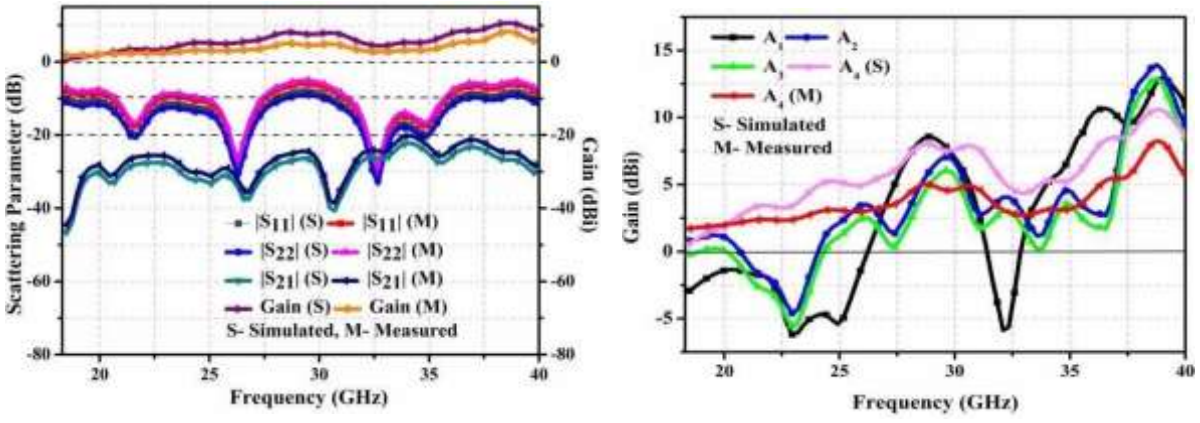

(a) (b)

Figure 6. Parametric analysis of the proposed antennas (A1–A4) showing (a) simulated and measured scattering parameters and (b) comparative gain performance

International Journal of Environmental Sciences
ISSN: 2229-7359
Vol. 11 No. 22s, 2025
https://theaspd.com/index.php

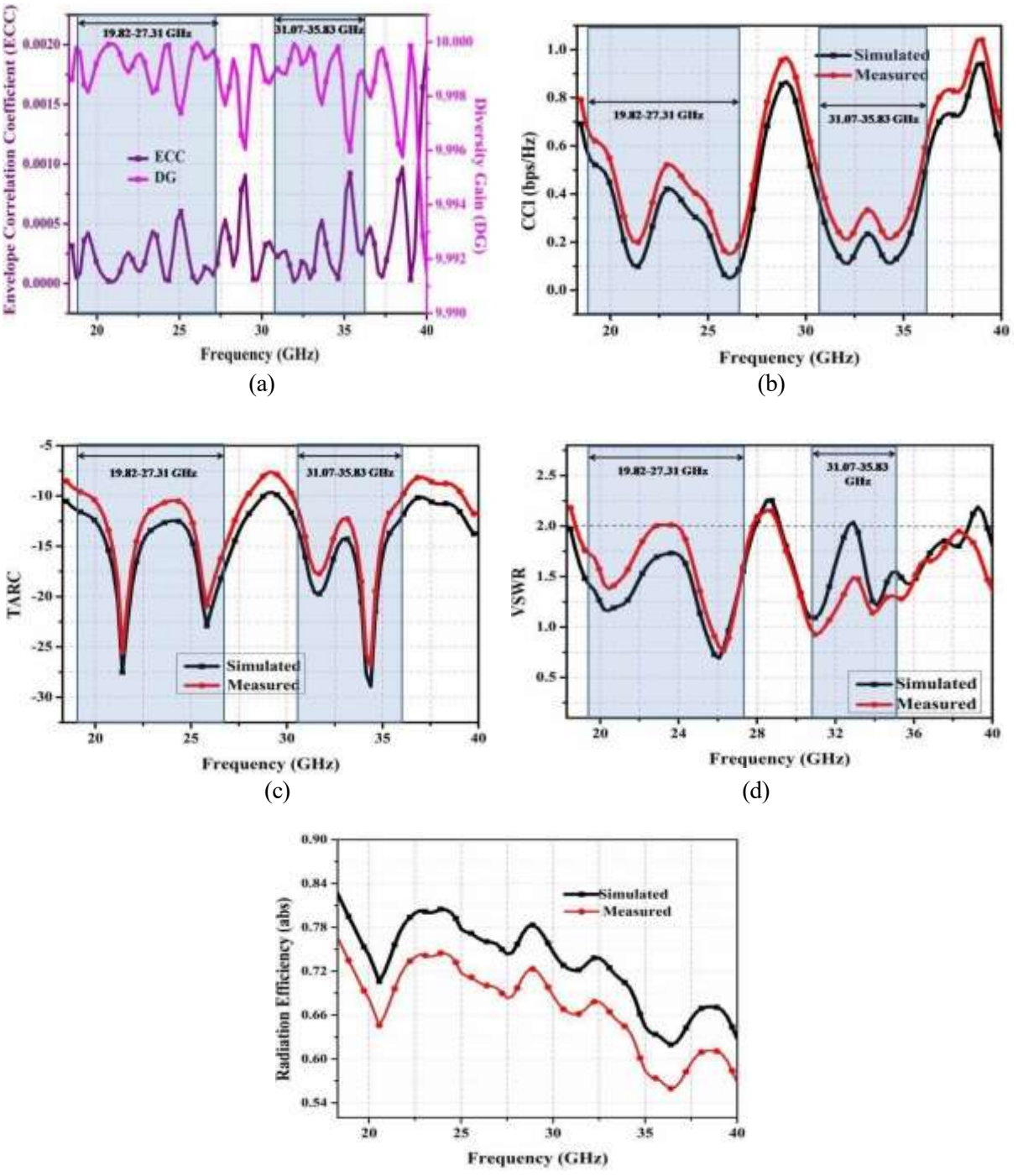

Figure 7. Performance analysis of the proposed antenna (A4), illustrating (a) Envelope Correlation Coefficient (ECC), (b) Channel Capacity Loss (CCL), (c) TARC, (d) Radiation Efficiency, and (e) VSWR, under both simulated and measured conditions.

A comparative study among antennas A1–A4 confirms that the proposed antenna (A4) exhibits superior performance in terms of impedance bandwidth (IBW), isolation, and gain. Specifically, antenna A4 achieves a peak gain of 5.2 dBi (simulated) and 5.0 dBi (measured) at Port-1, corresponding to the resonant frequencies of 26.29 GHz and 32.64 GHz (cf. Figure 6 and Table 1).

3.1 Performance Parameters

In this section, the diversity performance metrics of the proposed MIMO antenna have been analyzed, including Envelope Correlation Coefficient (ECC), Diversity Gain (DG), Total Active Reflection Coefficient (TARC), and Channel Capacity Loss (CCL), computed using MATLAB simulations.

The Envelope Correlation Coefficient (ρ) is a key parameter that indicates the degree of correlation between multiple antenna elements. Its value ranges between 0 and 1, where ρ = 1 signifies identical polarization with highly correlated radiation patterns**,** and ρ = 0 represents completely uncorrelated and distinct radiation patterns—typically achieved through orthogonal polarization. An ideal ECC value close to 0 indicates superior isolation between antenna elements, thereby enhancing the overall performance of MIMO systems.

The ECC can be derived using either the radiation patterns or the scattering parameters of the antenna. As reported in [35], the measured and simulated ECC of the proposed antenna is computed by employing both the S-parameters and far-field radiation characteristics, as defined in Equations (7) and (8).

$$E_{CC}^{ij} = \frac{|S^{*}S_{ii\ ij} + S^{*}S_{ji\ jj}|}{(1 - |S_{ii}|^{2} - |S_{ji}|^{2})\,(1 - |S_{jj}|^{2} - |S_{ij}|^{2})} \tag{7}$$

$$ECC = \frac{|f_{4\pi} f_1(\theta,\phi) \cdot f_2(\theta,\phi) d\Omega|^2}{\int_{4\pi} |f_1(\theta,\phi)|^2 d\Omega \cdot \int_{4\pi} |f_2(\theta,\phi)|^2 d\Omega} \tag{8}$$

In this analysis, $F_1(\theta, \phi)$ represents the electric field component when element 1 is excited while element 2 is terminated with a matched load. Conversely, $F_2(\theta, \phi)$ denotes the electric field component when element 2 is excited and element 1 is terminated with the corresponding load.

Another critical parameter for evaluating MIMO antenna performance is the Diversity Gain (DG). Within the operating bandwidth, an effective MIMO antenna should exhibit a high DG value, ideally close to 10 dB. DG quantifies the improvement in transmission reliability and reduction in power loss achieved through diversity techniques [37–38].

For the proposed MIMO antenna (A4), the DG fluctuates around 9.98 dB across both operating bands, as illustrated in Figure 7(a). The DG can be mathematically derived from the ECC using Equation (15).

In addition, Channel Capacity Loss (CCL) is another essential parameter that reflects the degradation in system capacity caused by mutual coupling effects. The simulated and measured CCL curves of the proposed antenna are shown in Figure 7(b). Based on the empirical formulations (Equations 9–12) provided in [23], the CCL value of the proposed design is computed, confirming its suitability for high-capacity MIMO applications.

$$\mathrm{CCL} = -\log_2(\det(\rho)) \tag{9}$$

$$\rho = \begin{bmatrix} \rho_{11} & \rho_{12} & \rho_{13} & \cdots & \rho_{18} \\ \rho_{21} & \rho_{22} & \rho_{23} & \cdots & \rho_{28} \\ \rho_{31} & \rho_{32} & \rho_{33} & \cdots & \rho_{38} \\ \vdots & \vdots & \vdots & \ddots & \vdots \\ \rho_{81} & \rho_{82} & \rho_{83} & \cdots & \rho_{88} \end{bmatrix} \tag{10}$$

$$\rho_{ii} = 1 - (|S_{ii}|^2 - |S_{ij}|^{-}) \tag{11}$$

$$\rho_{ij} = -(S_{ii}S_{ij} - S_{ji}S_{jj}^{*}) \tag{12}$$

The Channel Capacity Loss (CCL) values, obtained from both simulated and measured results, remain well below the acceptable limit of 0.25 bits/s/Hz [13]. This indicates minimal system capacity degradation, confirming that the proposed antenna maintains low mutual coupling between its ports. Consequently, it is highly suitable for high-data-rate MIMO communication systems, where reduced inter-port interference is essential for reliable performance.

The Diversity Gain (DG) further enhances system robustness by maximizing the signal-to-noise ratio (SNR) without requiring additional input power. This is achieved by selecting the strongest available signal, thereby mitigating the adverse effects of multipath fading. As defined in Equation (13) and detailed in [23], DG provides a quantitative measure of this improvement.

As illustrated in Figure 13, the proposed MIMO antenna exhibits excellent diversity characteristics, with DG values consistently remaining close to the ideal 10 dB across the entire operating frequency range. This demonstrates the antenna's effectiveness in supporting stable and efficient wireless communication links.

$$\mathrm{DG} = 10\sqrt{1 - (ECC^{i,j})^{2}} \tag{13}$$

he Channel Capacity Loss (CCL) is a crucial parameter for determining the maximum data rate at which information can be reliably transmitted over a communication channel without interruption. It is derived using the S-scattering parameters [29]. For the proposed MIMO antenna (A4), the CCL values are computed using Equation (9). The results demonstrate that the CCL remains below the acceptable threshold, with simulated values of 0.21 bits/s/Hz and measured values of 0.25 bits/s/Hz, across both operating bands (cf. Figure 7-b). This confirms that the antenna design ensures minimal system capacity degradation, making it highly efficient for high-data-rate wireless communication.

In addition, the Total Active Reflection Coefficient (TARC) has been analyzed for the proposed 2-port MIMO antenna. TARC is a key metric for evaluating how the excitation of one antenna element influences the overall performance of the other elements in the system [40–41]. A TARC value below 10 dB, observed in both simulated and measured results across the entire frequency band (cf. Figure 7-c), indicates superior efficiency with reduced signal reflections.

Mathematically, TARC for a dual-port configuration can be determined its detailed formulation for multi-port systems is expressed by Equation (14), as reported in [24–33]. A lower TARC signifies enhanced impedance matching, improved isolation, and better diversity characteristics, ultimately leading to higher efficiency and superior MIMO performance.\

$$\mathrm{TARC} = \frac{\sqrt{\left|\sum_{i=1}^{N} S_{i1} + \sum_{m=2}^{N} S_{im} e^{j\theta m-1}\right|}}{\sqrt{N}} \tag{14}$$

The Voltage Standing Wave Ratio (VSWR) of the proposed MIMO antenna (A4) has been both simulated and measured, as illustrated in Figure 7-d. Across the operating frequency range, the VSWR consistently remains below the threshold value of 2, confirming that the antenna is well-suited for practical applications. Specifically, at the resonant frequency of 26.29 GHz, the simulated and measured VSWR values are 1.55 and 1.52, respectively, within the frequency range of 19.82–27.31 GHz. Similarly, at the resonant frequency of 32.64 GHz, the simulated and measured VSWR values are 1.55 and 1.52, respectively, within the frequency range of 31.07–35.83 GHz. A VSWR of 2:1 is generally accepted as the benchmark for good antenna performance, and the obtained results confirm excellent impedance matching of the proposed design.

The radiation efficiency (RE) of the proposed antenna is presented in Figure 7-e. The measured and simulated results demonstrate maximum efficiencies of 78% (simulated) and 66% (measured) at the resonant frequencies of 26.29 GHz and 32.64 GHz, ensuring stable performance across the operating bands.

Furthermore, the 2D gain of the antenna, derived from the measured radiation pattern data, is illustrated in Figure 9. The measured gain values have been calculated using the Friis transmission equation (15 & 16), as detailed in [40]. These results further validate the robustness and high performance of the proposed antenna in terms of gain and radiation characteristics.

$$\text{Received power } (P_{rp}) = \left(\frac{\lambda_0}{4\pi R_d}\right)^{2} G_{rg} G_{tg} P_{tp} \tag{15}$$

$$\text{Far - field distance } (R_d) = \frac{2r^2}{\lambda_0} \tag{16}$$

Where r is the distance between the between (T_x) and (R_x) antennas, λ_0-wavelength, P_{tp}-transmitted power, G_{rg}&G_{tg} - is the received and transmitted gain.

The proposed antenna (A4) demonstrates both co- and cross-polarization patterns (simulated and measured) in the E-plane and H-plane, where the elevation axis of the antenna coordinate system

coincides with the polar axis (θ = 0°). During measurements, the elevation positioner was rotated from –180° to +180° in steps of 5°. Simulations were carried out using HFSS software, and corresponding measurements were formed in an anechoic chamber. Minor discrepancies between simulated and measured results can be attributed to the chamber's supporting hardware and the gain accuracy of the standard reference antenna used in the experiments.

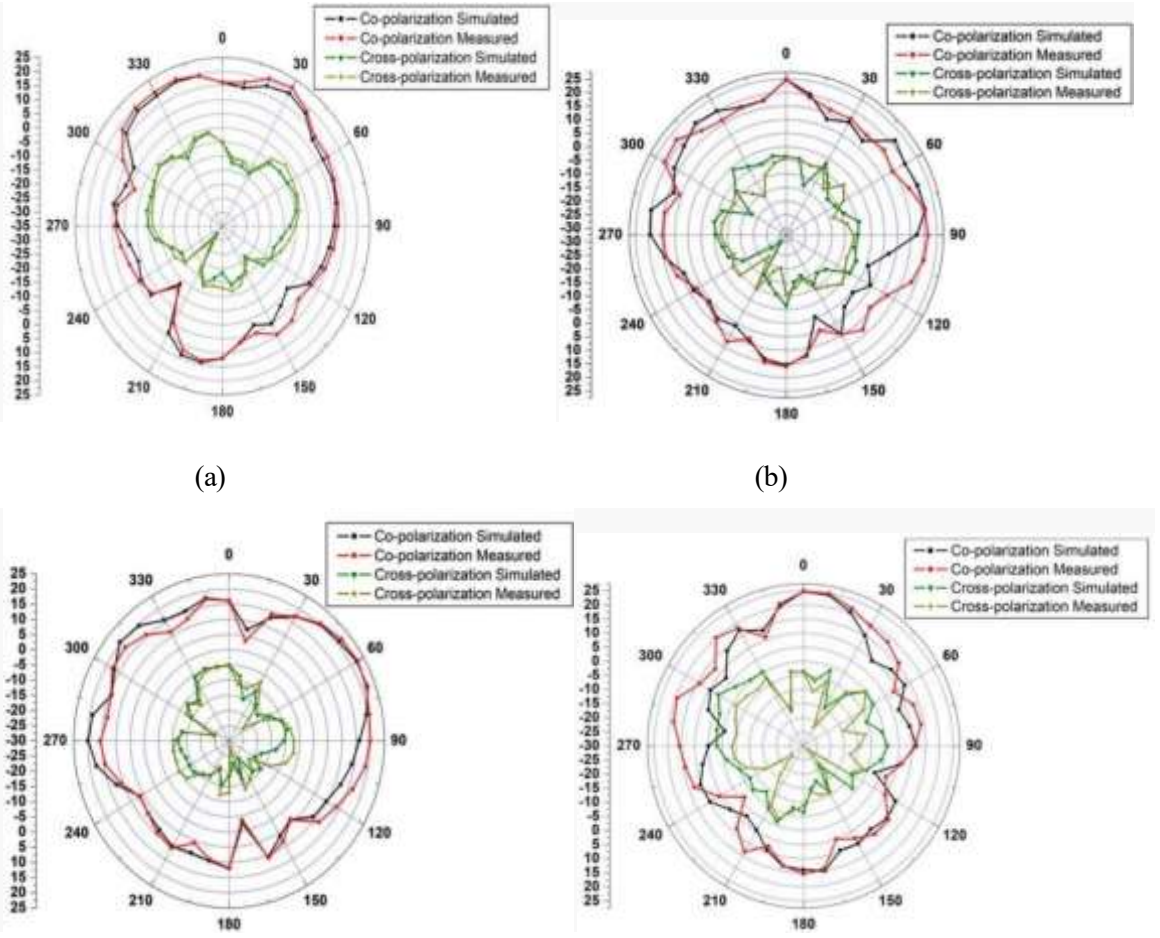

Figure 8. Co-polarization and cross-polarization characteristics (simulated and measured) of the proposed antenna design: (a) E-plane at 26.29 GHz, (b) H-plane at 26.29 GHz, (c) E-plane at 32.64 GHz, and (d) H-plane at 32.64 GHz.

As illustrated in Figure 8, the recommended antenna (A4) achieves a nearly omnidirectional radiation pattern with wide angular coverage, thereby enhancing the polarization performance and improving signal reception. Although cross-polarization components are generally undesirable in MIMO systems as they may introduce uncertainty, the achieved suppression level of 10–15 dB is considered sufficient for reliable operation.

4. CONCLUSION

This work presents a compact spiral-shaped MIMO antenna (A4) with an integrated meander-line structure and parallel configuration to achieve dual-band resonance. The proposed antenna effectively operates over 19.82–27.31 GHz (K-band: 18–26.25 GHz) and 31.07–35.83 GHz (Ka-band: 26.5–40 GHz). Both simulated and measured results confirm excellent performance, with port-to-port isolation consistently better than –30 dB across the operating bands, thereby ensuring minimal mutual coupling. The designed MIMO antenna (A4) demonstrates enhanced stability at higher data rates, improved efficiency, and reliable wideband coverage, making it well-suited for next-generation wireless systems. Its dual-band operation, wide impedance bandwidth, and strong isolation capabilities render it highly

promising for 5G (n258), satellite communications, and other advanced wireless applications requiring high spectral efficiency and low interference.

Future work may focus on further improving bandwidth enhancement techniques and isolation optimization to extend the antenna's potential for emerging opportunity-driven wireless technologies.

REFERENCES

[1] C. Liang, R. Su, P. Gao, and P. Wang, "Compact printed MIMO antenna with 6.1 GHz notched band for ultra-wideband applications," Progress In Electromagnetics Research Letters, vol. 76, pp. 77–83, 2018.

[2] M. S. Khan, A. Iftikhar, R. M. Shubair, A. D. Capobianco, B. D. Braaten, and D. E. Anagnostou, "A four element, planar, compact UWB MIMO antenna with WLAN band rejection capabilities," Microwave and Optical Technology Letters, vol. 62, no. 10, pp. 3124–3131, 2020.

[3] T. Govindan, S. K. Palaniswamy, M. Kanagasabai, and S. Kumar, "Design and analysis of UWB MIMO antenna for smart fabric communications," International Journal of Antennas and Propagation, 2022.

[4] A. Wu, M. Zhao, P. Zhang, and Z. Zhang, "A compact four-port MIMO antenna for UWB applications," Sensors, vol. 22, no. 15, p. 5788, 2022.

[5] O. Sokunbi, H. Attia, A. Hamza, A. Shamim, Y. Yu, and A. A. Kishk, "New self-isolated wideband MIMO antenna system for 5G mm-wave applications using slot characteristics," IEEE Open Journal of Antennas and Propagation, vol. 4, pp. 81–90, 2023.

[6] N. El Idrissi, D. Kumutha, S. Jeevitha, and S. Das, "A compact multi-resonant wideband MIMO antenna for 5G communication systems at mm-wave band," Journal of Nano- and Electronic Physics, vol. 15, no. 1, 2023.

[7] H. Parikh, S. Pandey, and M. Sahoo, "Design of a modified E-shaped dual band patch antenna for Ku-band application," in Proc. Int. Conf. Communication Systems and Network Technologies (CSNT), pp. 49–52, IEEE, 2012.

[8] T. N. Thi, K. Hwang, and H. Kim, "Dual-band circularly-polarised spidron fractal microstrip patch antenna for Ku-band satellite communication applications," Electronics Letters, vol. 49, no. 7, pp. 444–445, 2013.

[9] A. Sayed, R. S. Ghonam, and A. Zekry, "Design of a compact dual band microstrip antenna for Ku-band applications," International Journal of Computer Applications, vol. 115, no. 13, 2015.

[10] M. Samsuzzaman, M. T. Islam, N. Misran, and M. A. M. Ali, "Dual band X-shape microstrip patch antenna for satellite applications," Procedia Technology, vol. 11, pp. 1223–1228, 2013.

[11] P. L. Vijayvergiya and R. K. Panigrahi, "Single-layer single-patch dual band antenna for satellite applications," IET Microwaves, Antennas & Propagation, vol. 11, no. 5, pp. 664–669, 2017.

[12] G. S. Saini and R. Kumar, "A low profile patch antenna for Ku-band applications," International Journal of Electronics Letters, vol. 9, no. 1, pp. 47–57, 2021.

[13] M.-Y. Li, Z.-Q. Xu, Y.-L. Ban, C.-Y.-D. Sim, and Z.-F. Yu, "Eight-port orthogonally dual-polarised MIMO antennas using loop structures for 5G smartphone," IET Microwaves, Antennas & Propagation, vol. 11, no. 12, pp. 1810–1816, 2017.

[14] A. Kumar, S. K. Mahto, and R. Sinha, "Y-shaped antenna for 5G enabled gadgets and its MIMO for smartphone applications," in Proc. URSI Regional Conf. on Radio Science (URSI-RCRS), pp. 1–4, IEEE, 2020.

[15] A. Kumar, S. K. Mahto, R. Sinha, and A. Choubey, "Dual circular slot ring triple-band MIMO antenna for 5G applications," Frequenz, vol. 75, no. 3–4, pp. 91–100, 2021.

[16] A. K. Singh, A. Pandey, P. K. Mishra, and R. S. Yadav, "A miniaturized 2×2 double flare horn shaped MIMO antenna with enhanced isolation for K and Ka band applications," Progress In Electromagnetics Research M, vol. 111, pp. 159–171, 2022.

[17] A. K. Singh, A. Pandey, S. Singh, V. Yadav, and R. S. Yadav, "Ringing phenomenon-based circularly polarized MIMO antenna for Ku/K band communication," Progress In Electromagnetics Research C, vol. 124, pp. 111–124, 2022.

[18] A. G. Alharbi et al., "Novel MIMO antenna system for ultra-wideband applications," Applied Sciences, vol. 12, no. 7, p. 3684, 2022.

[19] T. Addepalli and V. R. Anitha, "Compact two-port MIMO antenna with high isolation using parasitic reflectors for UWB, X and Ku band applications," Progress In Electromagnetics Research C, vol. 102, pp. 63–77, 2020.

[20] M. Job, A. Pandey, P. Yadav, and R. Yadav, "Tri-forked dual-port MIMO antenna for Ku/K-band radar and satellite applications," Semiconductor Optoelectronics, vol. 41, no. 11, pp. 587–598, 2022.

[21] A. K. Singh, A. Pandey, S. Singh, V. Yadav, and R. Singh, "Quad-port circularly polarized MIMO antenna for K band applications," in Proc. Int. Conf. Communication and Electronics Systems (ICCES), Coimbatore, India, pp. 405–410, 2021.

[22] A. K. Singh et al., "A compact MIMO antenna for 5G NR frequency bands n257/n258/n261 under millimeter-wave communication," IETE Journal of Research, pp. 1–13, 2022.

[23] H. Jiang, L.-M. Si, W. Hu, and X. Lv, "A symmetrical dual-beam bowtie antenna with gain enhancement using

metamaterial for 5G MIMO applications," IEEE Photonics Journal, vol. 11, no. 1, pp. 1–9, 2019.

[24] M. Khalid et al., "4-port MIMO antenna with defected ground structure for 5G millimeter wave applications," Electronics, vol. 9, no. 1, p. 71, 2020.

[25] B. T. Ahmed and I. F. Rodríguez, "Compact high isolation UWB MIMO antennas," Wireless Networks, vol. 28, no. 5, pp. 1977–1999, 2022.

[26] A. Iqbal, O. A. Saraereh, A. W. Ahmad, and S. Bashir, "Mutual coupling reduction using F-shaped stubs in UWB-MIMO antenna," IEEE Access, vol. 6, pp. 2755–2759, 2017.

[27] A. Pandey, A. K. Singh, S. Singh, R. Singh, and B. Mishra, "Quad-band MIMO antenna for radar and satellite applications," in VLSI, Microwave and Wireless Technologies: Select Proceedings of ICVMWT 2021, pp. 317–327, Springer, 2022.

[28] A. Pandey, J. A. Ansari, I. Masroor, and P. K. Mishra, "Quad-element penta-band MIMO antenna for 5G millimeter-wave applications," in Emerging Technology Trends in Electronics, Communication and Networking (ET2ECN 2021), pp. 73–83, Springer, 2022.

[29] M. S. Sharawi, S. K. Podilchak, M. T. Hussain, and Y. M. Antar, "Dielectric resonator based MIMO antenna system enabling millimetre-wave mobile devices," IET Microwaves, Antennas & Propagation, vol. 11, no. 2, pp. 287–293, 2017.

[30] G. Saxena, P. Jain, and Y. K. Awasthi, "High diversity gain super-wideband single band-notch MIMO antenna for multiple wireless applications," IET Microwaves, Antennas & Propagation, vol. 14, no. 1, pp. 109–119, 2020.

[31] G.-S. Lin, C.-H. Sung, J.-L. Chen, L.-S. Chen, and M.-P. Houng, "Isolation improvement in UWB MIMO antenna system using carbon black film," IEEE Antennas and Wireless Propagation Letters, vol. 16, pp. 222–225, 2016.

[32] Y. K. Choukiker, S. K. Sharma, and S. K. Behera, "Hybrid fractal shape planar monopole antenna covering multiband wireless communications with MIMO implementation for handheld mobile devices," IEEE Transactions on Antennas and Propagation, vol. 62, no. 3, pp. 1483–1488, 2013.

[33] A. K. Singh, A. K. Dwivedi, K. N. Nagesh, V. Singh, and R. S. Yadav, "Compact 4-port planar MIMO antenna with enhanced isolation for WLAN/WiMAX applications," Sādhanā, vol. 47, no. 3, p. 138, 2022.

[34] S. Kumar, R. Kumar, R. K. Vishwakarma, and K. Srivastava, "An improved compact MIMO antenna for wireless applications with band-notched characteristics," AEU–International Journal of Electronics and Communications, vol. 90, pp. 20–29, 2018.

[35] Q. Li, D. Song, C. Yuan, and W. Nie, "An image recognition method for the deformation area of open-pit rock slopes under variable rainfall," Measurement, vol. 188, p. 110544, 2022.

[36] A. Kumar, A. K. Dwivedi, A. Sharma, A. K. Pandey, and V. Singh, "Circularly polarised dielectric resonator based two port filtenna for millimeter-wave 5G communication system," IETE Technical Review, vol. 39, no. 6, pp. 1501–1511, 2022.

[37] A. Toktas, "G-shaped band-notched ultra-wideband MIMO antenna system for mobile terminals," IET Microwaves, Antennas & Propagation, vol. 11, no. 5, pp. 718–725, 2017.

[38] A. K. Dwivedi, A. Sharma, A. K. Pandey, and V. Singh, "Two port circularly polarized MIMO antenna design and investigation for 5G communication systems," Wireless Personal Communications, vol. 120, no. 3, pp. 2085–2099, 2021.